STOCHASTICITY AND RESONANCES IN THE TWO BEAM ACCELERATOR

by

N. W. Murray and M. A. Lieberman

Memorandum No. UCB/ERL M86/76

26 September 1986

STOCHASTICITY AND RESONANCES IN THE TWO BEAM ACCELERATOR

by

N. W. Murray and M. A. Lieberman

Memorandum No. UCB/ERL M86/76

26 September 1986

ELECTRONICS RESEARCH LABORATORY

College of Engineering
University of California, Berkeley
94720

STOCHASTICITY AND RESONANCES IN THE TWO BEAM ACCELERATOR

by

N. W. Murray and M. A. Lieberman

Memorandum No. UCB/ERL M86/76

26 September 1986

ELECTRONICS RESEARCH LABORATORY

College of Engineering
University of California, Berkeley
94720

STOCHASTICITY AND RESONANCES IN THE TWO BEAM ACCELERATOR

N. W. Murray and M. A. Lieberman
Department of Electrical Engineering and
Computer Sciences and the
Electronics Research Laboratory,
University of California, Berkeley, CA 94720

ABSTRACT

The two beam accelerator is a proposed linear e^+e^- machine employing 2×500 tapered free electron lasers (FELs) as a source of microwave power. A high current, low energy (20 MeV) beam drives the FELs, producing 1 cm microwaves. These microwaves are used to accelerate a low current beam to energies of 1 TeV. High efficiencies are obtained by re-accelerating the low energy beam after passing through each FEL. Restoring the 2 MeV/particle lost on passing through each FEL section (using an induction accelerator) avoids wasting the 18 MeV/particle left in the beam. The periodic nature of the acceleration and deceleration of the low energy beam can lead to stochastic motion. We exhibit design criteria that ensure that detrapping of the low energy beam by this stochasticity is minimal, preserving the high efficiencies inherent in a single tapered FEL. Numerical integrations of a one dimensional model for the FELs are presented showing various degrees of detrapping. We also explore the effects of islands produced by resonances between the periodic acceleration and the trapped particle motion. These islands represent coherent motion of large numbers of trapped particles, leading to oscillations in the power output of the FELs.

INTRODUCTION

In their search for an understanding of the fundamental structure of matter, high energy physicists have been the driving force behind the development of accelerator technology. Presently, the goal is to study interactions at energies of a few TeV (10^{12}eV). Historically, the results of high energy experiments have stimulated interest in phenomena at still higher energies, and there is no reason to believe that this trend will not continue. Today's accelerators rely on well understood and well tested techniques to produce accelerating gradients of about 20 MeV per meter. To accelerate particles to 1 TeV then requires very large machines, typically tens of kilometers in circumference or length. The cost of such large devices is becoming prohibitive.

We briefly review three state-of-the art machines. The proposed superconducting super collider (SSC) is a proton-proton collider using a standard colliding ring configuration. Two proton beams are circulated in opposite directions in the ring. The center of mass energy in a collision is 40 TeV. Individual protons are known to consist of many partons, each of which carries only a fraction of the proton's energy. Thus the average center-of-mass energy for a parton-parton collision is much less than the apparent center-of-mass energy of the proton-proton collision. For this reason as well as others protons are not ideal candidates for studying high energy physics[1].

Electron positron colliding beam storage rings such as the large electron positron ring at CERN (LEP) avoid these problems. At presently attainable energies electrons do not display any internal structure. The center of mass energy of the two beams is the center of mass energy available in a collision; for LEP the design energy is 200 GeV. However, energy losses due to synchrotron radiation are much higher for an electron ring than for a proton ring of the same radius. To keep synchrotron losses to acceptable levels LEP was built 27 km in circumference. To scale up LEP to a 1×1 TeV machine would require the purchase of large amounts of real estate. Large $e^+ e^-$ machines are simply too costly to build.

Linear colliders, such as the Stanford Linear Collider (SLC), may prove the successors to colliding beam storage rings. To avoid very long linear machines, which encounter the same fiscal constraints as very large ring machines, large accelerating gradients are necessary . The accelerating gradient at SLC is roughly 20 MeV/m, running with a 10 cm wavelength. Thus a 1.5 on 1.5 TeV machine using the SLC technology would be 2×50 km long.

The accelerating gradient may be improved by increasing the strength of the electric field E. Unfortunately, very high electric fields cause breakdown (sparks) in the accelerating structure. This is the limiting factor at SLC. Furthermore, increasing E will increase the energy stored in the machine. Maintaining stored energy requires (expensive) power, so increasing the electric field without changing the rest of the design is costly.

Both of these problems can be eased by using shorter wavelengths[2,3,4]. The breakdown field scales as $\lambda^{-7/8}$ and the stored energy required for a given accelerating gradient scales as λ^2. If one could run an accelerator using a wave length of 1 cm then accelerating gradients of several hundred MeV/m could be obtained with acceptable power costs. Unfortunately, klystrons such as those employed at SLC are not efficient generators of 1 cm power.

Sessler[3] noted that free electron lasers (FELs) can efficiently generate 1 cm power and proposed the Two Beam Accelerator (TBA). In this scheme about 500 FELs replace the klystrons. The FELs are powered by a single low energy, high current electron beam. This high current beam propagates parallel to the relatively low current beam that is to be accelerated to high energy. The microwave power generated by the FELs is coupled into the accelerating

structure in the same manner as is the power generated by klystrons in present linear accelerators.

The energy extracted from the low energy beam in the form of microwaves must be replaced periodically if the beam is to be used to power more than a few meters of high gradient acceleration. Conventional induction units would accomplish this. The acceleration of low energy, high current beams by induction units is a well developed, efficient technology.

Considerable analysis of the TBA must be done to determine its feasibility and to identify design criteria that a successful candidate must meet. For example, the coupling scheme between the two beams must be developed and studied. The growth of any side band instabilities in the FELs must be suppressed. These and other considerations are being examined[5,6].

In this study we will examine the question of particle detrapping in the low energy beam due to stochasticity. A non-autonomous one degree of freedom Hamiltonian is used to describe the motion of an electron in the FEL due to the ponderomotive force of the wave and FEL wiggler field. Resonances between this motion and the spatial variation along the series of FELs form islands which may overlap. The stochasticity generic to such systems may cause the low energy beam to disintegrate, preventing acceleration of the high energy beam. We develop criteria to ensure that this does not occur.

In the next section we write down the equations of motion for the electrons in the FEL and derive a Hamiltonian that generates them. An analysis of this Hamiltonian allows us to select an optimum design for the FEL wiggler. In Section we obtain an estimate for the size of the trapped region from a surface-of-section mapping. The results are compared to numerical integrations of the equations. In Section we describe the effects of resonances between the libration in the ponderomotive well of the FEL and the periodic driving of the induction unit. These resonances can lead to the coherent libration of a significant fraction of the trapped particle population. We believe that these resonances explain the bunching effect observed by Sternbach and Sessler[7].

HAMILTONIAN FORMULATION

A model of the low energy beam dynamics of the TBA is shown in Fig. 1. The low energy beam periodically passes through a tapered wiggler free electron laser which extracts a fraction of its energy as microwave power to accelerate the high energy beam. The low energy beam then passes through an induction unit which restores the beam to its original energy. Current schemes call for about 500 FELs for each accelerator.

Kroll, Morton and Rosenbluth[8] discuss the operation of tapered wiggler FELs. In an FEL, electrons pass through a periodic transverse magnetic field, called the wiggler field. The resulting acceleration causes the electrons to emit or absorb electromagnetic waves. Since the electrons travel with a velocity less

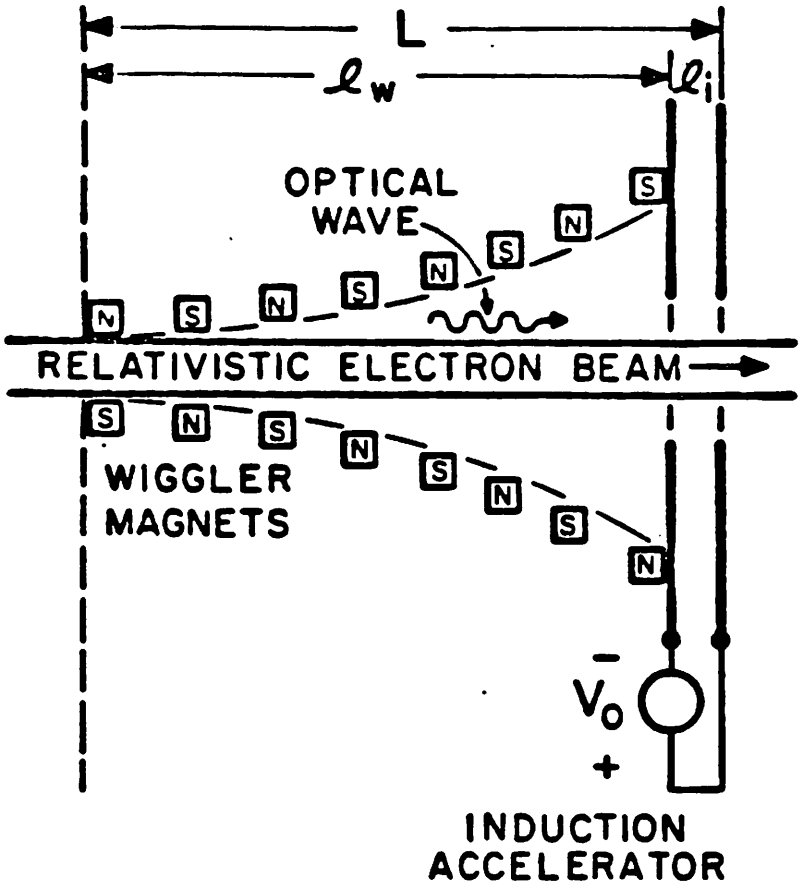

Figure 1: One section of the TBA, consisting of a tapered free electron laser followed by an induction acceleration unit. In this paper we assume an infinitely thin induction acceleration region so that $l_i \to 0$.

than the speed of light, they will not, in general, stay in phase with the wave. If the electrons fall behind the wave by an integer number of wavelengths while travelling a distance equal to the period of the magnetic field, they will interact coherently with the wave. An FEL operates in such a manner as to ensure that most of the beam electrons emit coherent radiation.

FEls with constant amplitude, constant wavelength wiggler fields cannot be steady state devices; the electrons give up energy to the electromagnetic wave and slow down. Their phase relative to the wave slips until they begin to reabsorb energy from the wave. Thus, electrons oscillate in energy, the wave amplitude growing when the electron energy decreases and vice versa. The motion of the electrons in the energy-phase angle phase space is similar to the motion of a pendulum, with electron libration around a stable center in phase space. The region of phase space inside the largest libration orbit is called a bucket. The maximum energy that may be extracted from the beam is some fraction of the width of the bucket in energy. In addition, the spread in energy of the emerging beam is of order the bucket size. Due to this spread in energy the beam cannot be used to power another FEL.

The tapered FEL avoids this limitation by slowly changing the strength and the period of the wiggler field along the beam path to ensure that the electrons on the average emit energy. Tapering the wiggler takes advantage of the fact that electrons are trapped in the bucket. The bucket is moved adiabatically down in energy drawing the trapped electrons down with it. The spread in energy of the beam is again of the order of the bucket height, but the tapered FEL can still extract energy from the beam.

For modeling the TBA, we assume that an electromagnetic wave has been produced previous to the start of steady state FEL operation. This could be accomplished by a series of FELs in which no power is drawn off to power the high gradient structure. Thus we assume that the field strength at the beginning of the FEL is non-zero.

We start with the equations of Kroll, Morton and Rosenbluth;

$$\begin{aligned}
\frac{d\gamma_i}{dz} &= -\frac{\omega_s a_s a_w}{c\gamma_i}\sin\psi_i, \\
\frac{d\psi_i}{dz} &= k_w + \frac{d\phi}{dz} - \frac{\omega_s}{c\gamma_i^2}(1 + a_w^2 - 2a_w a_s\cos\psi_i), \\
\frac{da_s}{dz} &= \frac{k_p^2 c}{2\omega_s} a_w \left\langle \frac{\sin\psi}{\gamma} \right\rangle, \\
\frac{d\phi}{dz} &= \frac{k_p^2 c a_w}{2\omega_s a_s} \left\langle \frac{\cos\psi}{\gamma} \right\rangle.
\end{aligned} \tag{1}$$

In these equations γ_i is the energy of the i'th particle and the conjugate variable ψ_i is the phase of the i'th particle in the ponderomotive well, defined by

$$\psi = \int_0^z (k_w(z) + k_s)dz' \; - \; \omega_s t \; . \tag{2}$$

The quantity k_w is the wavenumber of the wiggler field, k_s and ω_s are the wavenumber and the frequency of the microwaves, and $a_s = eA_s/mc^2$ is the dimensionless vector potential of the wave (the subscript s stands for signal). The quantity $\phi = \int k_s dz - \omega_s t$ is the phase of the wave, a_w is the dimensionless vector potential of the wiggler magnetic field, having wave number k_w, and $k_p = 4\pi n_e e^2/mc$ is the plasma wave number. The independent variable z is the distance along the beam path. The brackets in the last two equations denote an average over all N particles in the beam.

In the TBA, the FELs will be in waveguides. The effect on equations (1) is minor[5]. In the second equation we must replace $k_w \rightarrow k_w - \delta k_s$, where $\delta k_s = \omega_s/c - k_s$ is the shift of the wavenumber from its value in vacuum. This has the effect of changing the numerical value of k_w. Similarly, k_p must be adjusted by a fill factor, $k_p^2 \rightarrow k_p^2$(beam area/mode area). Again, this means that the numerical value of k_p must be adjusted from its value in vacuum.

In terms of the wave action $J_w = N(\omega_s^2/k_p^2c^2)a_s^2$ and letting $\theta_i = \psi_i - \chi$ where $\chi = -\phi$, we obtain from (1)

$$\begin{aligned}
\frac{d\gamma_i}{dz} &= -k_p a_w \left(\frac{J_w}{N}\right)^{1/2} \frac{\sin(\theta_i - \chi)}{\gamma_i}, \\
\frac{d\theta_i}{dz} &= k_w - \frac{\omega_s}{2c\gamma_i^2}(1 + a_w^2) + \frac{k_p a_w}{\gamma_i^2}\left(\frac{J_w}{N}\right)^{1/2} \cos(\theta_i - \chi), \\
\frac{dJ_w}{dz} &= k_p a_w \left(\frac{J_w}{N}\right)^{1/2} \sum_i \frac{\sin(\theta_i - \chi)}{\gamma_i}, \\
\frac{d\chi}{dz} &= -\frac{k_p a_w}{2}\left(\frac{J_w}{N}\right)^{-1/2} \frac{1}{N} \sum_i \frac{\cos(\theta_i - \chi)}{\gamma_i}.
\end{aligned} \tag{3}$$

These equations may be derived from the Hamiltonian

$$\begin{aligned}
H(\gamma_i, \theta_i; J_w, \chi) = \sum_i \Bigg\{ & k_w \gamma_i + \frac{\omega_s}{2c\gamma_i}(1 + a_w^2) - \\
& \frac{a_w k_p}{\gamma_i}\left(\frac{J_w}{N}\right)^{1/2} \cos(\theta_i - \chi) \Bigg\}.
\end{aligned} \tag{4}$$

We expect that the total energy E, i.e. the wave energy plus the particle energy, will be a constant of the motion. Summing the first and third equations of (3) confirms that this is the case. Because of this it is convenient to make a canonical transformation to $E = J_w + \sum_i \gamma_i$. We use the generating function $F_2(p_i, \theta_i; E, \chi) = \chi(E - \sum_i p_i) + \theta_i p_i$ to obtain $J_w = E - \sum_i p_i$, $\gamma_i = p_i$, $\bar{\chi} = \chi$, and $\bar{\theta}_j = \theta_j - \chi$. This leads to the Hamiltonian

$$H_e(p_i, \theta_i; E, \chi) = \sum_i \left\{ k_w p_i + \frac{\omega_s}{2cp_i}(1 + a_w^2) - \frac{k_p a_w}{p_i} \frac{\left(E - \sum_j p_j\right)^{1/2}}{N^{1/2}} \cos\bar{\theta}_i \right\}. \tag{5}$$

Note that $\bar{\theta}_i = \psi_i$ and $p_i = \gamma_i$, so we use ψ and γ_i. Since χ does not appear in the Hamiltonian the total energy E is constant.

Setting the derivatives of the Hamiltonian with respect to γ and ψ equal to zero, we find the two conditions for resonance

$$\begin{aligned} k_w + \frac{d\phi}{dz} - \frac{1}{2}\frac{\omega_s(1+a_w^2)}{c\gamma_r(z)^2} + \frac{k_p a_w (E - N\gamma_r)^{1/2}}{\gamma_r^2 N^{\frac{1}{2}}} cos\psi_r = 0 \,, \\ \frac{d\gamma_r(z)}{dz} = -\frac{k_p a_w}{\gamma_r(z)}\frac{(E - N\gamma_r)^{1/2}}{N^{1/2}} \sin\psi_r \,, \end{aligned} \tag{6}$$

which yields the resonance values γ_r and ψ_r. Since we are interested in studying the motion of particles in the bucket we make a final canonical transformation to coordinates around the resonance. The generating function $F_2(\bar{\gamma}_i, \psi_i; \bar{E}, \chi) = \bar{E}\chi + (\bar{\gamma}_i + \gamma_r(z))\psi_i - \bar{\gamma}_i\psi_r$ gives us the new Hamiltonian

$$\begin{aligned} \bar{H} = \sum_{i=1}^{N}\Big\{ & k_w(\gamma_r + \bar{\gamma}_i) + \frac{\omega_s}{2c(\gamma_r + \bar{\gamma}_i)}(1 + a_w^2) \\ & - k_p a_w \frac{(E - N\gamma_r - \sum_{j=1}^{N}\bar{\gamma}_j)^{1/2}}{N^{1/2}(\gamma_r + \bar{\gamma}_i)} \cos(\psi_r + \bar{\psi}_i) + \frac{d\gamma_r}{dz}\bar{\psi}_i \Big\}. \end{aligned} \tag{7}$$

The new variable $\bar{\gamma}_i$ is the deviation of the energy of the i'th particle from the resonant value γ_r.

Finally, we make the assumption that $N\gamma_r >> \sum_{j=1}^{N}\bar{\gamma}_i$ or $\gamma_r >> < \bar{\gamma}_i >$. We expect that the particles will be evenly distributed within the bucket so that $< \bar{\gamma}_i > \approx 0$. In reference[8] this corresponds to $k_w >> d\phi/dz$, $\omega_s a_w^2/(2c\gamma_i^2) >> (d\phi/dz)$, since $(d\phi/dz)$ is nearly constant. This decouples the equations for γ and ψ from the equation for ϕ. Using this approximation and dropping the bars over the particle energy and phase

$$\begin{aligned} H = \sum_{i=1}^{N}\Big\{ & k_w(\gamma_r + \gamma_i) + \frac{\omega_s}{2c(\gamma_r + \gamma_i)}(1 + a_w^2) - \\ & \frac{k_p a_w}{(\gamma_r + \gamma_i)}\frac{(E - N\gamma_r)^{1/2}}{N^{1/2}} \cos(\psi_r + \psi_i) + \frac{d\gamma_r}{dz}\psi_i \Big\} \\ = \sum_{i=1}^{N} H_i \,. \end{aligned} \tag{8}$$

The corresponding equations of motion are

$$\begin{aligned}
\frac{d\gamma_i}{dz} &= -\frac{k_p a_w}{(\gamma_r+\gamma_i)}\frac{(E-N\gamma_r)^{1/2}}{N^{1/2}}\sin(\psi_r+\psi_i) - \frac{d\gamma_r}{dz}, \\
\frac{d\psi_i}{dz} &= k_w - \frac{\omega_s}{2c(\gamma_r+\gamma_i)^2}(1+a_w^2) + \frac{k_p a_w}{(\gamma_r+\gamma_i)^2}\frac{(E-N\gamma_r)^{1/2}}{N^{1/2}}\cos(\psi_r+\psi_i), \\
\frac{dE}{dz} &= 0, \\
\frac{d\phi}{dz} &= -\frac{k_p a_w}{2(E-N\gamma_r)^{1/2}N^{1/2}}\sum_{i=1}^{N}\frac{\cos(\psi_r+\psi_i)}{(\gamma_r+\gamma_i)}.
\end{aligned} \tag{9}$$

Since different particles are decoupled we will drop the subscript i. For the TBA a_w, γ_r and E are periodic functions of z, e.g. $a_w(z+L) = a_w(z)$, where L is the length of an FEL making up one section of the TBA.

Using the Hamiltonian (8) we would like to design an FEL so that the area of the trapped region in phase space is a maximum. We have several parameters at our disposal: the wiggler strength as a function of z, $a_w(z)$, the wiggler wavelength $k_w(z)$, and the amplitude of the signal $a_s(z)$, or,equivalently the total energy $E(z)$. We will choose a linear dependence for $\gamma_r(z)$ for simplicity. We have shown that in an FEL with no power extracted E is a constant of the motion. However in the TBA we wish to extract energy from the device, in this case by placing ports in the FELs. This may be modeled in the Hamiltonian (8) simply by adding a term $f(z)\chi$ where $f(z)$ is the derivative of the desired z dependence of E. To motivate our design choices consider the expansion of H in powers of γ/γ_r:

$$\begin{aligned}
H &= H(0,\psi,E,\chi) + \left.\frac{\partial H}{\partial\gamma}\right|_0\gamma + \frac{1}{2}\left.\frac{\partial^2 H}{\partial\gamma^2}\right|_0\gamma^2 + \cdots \\
&= k_w\gamma_r + \frac{1}{2}G(z)\gamma_r^2 - F_o(z)\cos(\psi_r+\psi) + \frac{d\gamma_r}{dz}\psi \\
&\quad + \left[k_w(z)\gamma_r - \frac{1}{2}G(z)\gamma_r^2 + F_o\cos(\psi_r+\psi)\right]\left(\frac{\gamma}{\gamma_r}\right) \\
&\quad + \left[\frac{1}{2}G(z)\gamma_r^2(z) - F_o\cos(\psi_r+\psi)\right]\left(\frac{\gamma}{\gamma_r}\right)^2 \\
&\quad - \left[\frac{1}{2}G(z)\gamma_r^2(z) - F_o\cos(\psi_r+\psi)\right]\left(\frac{\gamma}{\gamma_r}\right)^3 \\
&\quad + \left[\frac{1}{2}G(z)\gamma_r^2(z) - F_o\cos(\psi_r+\psi)\right]\left(\frac{\gamma}{\gamma_r}\right)^4 \\
&\quad + O\left(\frac{\gamma}{\gamma_r}\right)^5,
\end{aligned} \tag{10}$$

where $G(z) = \omega_s(1+a_w^2)/(c\gamma_r^3)$ and $F_o = \omega_s a_w a_s/(c\gamma_r)$.

Using the resonance conditions (6) and ignoring terms that are independent of γ and ψ, the Hamiltonian (10) simplifies to

$$\begin{aligned} H =& \frac{1}{2}G(z)\gamma^2 - F_o\cos\psi_r\cos\psi + \frac{F_o\sin\psi_r}{\gamma_r(z)}\gamma\sin\psi \\ &+ F_o\sin\psi_r(\sin\psi-\psi) + \frac{F_o\cos\psi_r}{\gamma_r(z)}(\cos\psi-1)\gamma \\ &+ F_o(\sin\psi_r\sin\psi-\cos\psi_r\cos\psi)\left(\frac{\gamma}{\gamma_r}\right)^2+\ldots. \end{aligned} \tag{11}$$

The Hamiltonian (11) has the form of a pendulum (the first two terms), plus perturbations. However, the "mass" $G(z)$ and the "length" $F(z) = F_o\cos\psi_r$ are both functions of the "time" z. If the variation with z is slow compared to the frequency $\sqrt{FG}$ adiabatic theory tells us that the action does not change, and particles are trapped. This is in fact the case as the particles pass through the slow taper of the FEL. We also assume that a_w and a_s do not vanish in the induction accelerator unit so that the separatrix defining the bucket does not collapse.

When the beam passes through the induction unit to the beginning of the next FEL section, k_w, a_w, γ_r and a_s or E all vary rapidly. This variation may break adiabaticity, causing detrapping of the electrons. To avoid this, we choose the functions a_w, k_w and E so that G and F are held constant. Specifically we set

$$\begin{aligned} \gamma_r(z) &= \gamma_0 - \Delta\gamma\frac{z}{L} \\ a_w(z) &= \sqrt{(1+a_w^2(0))\left(\frac{\gamma_r}{\gamma_0}\right)^3 - 1}. \\ k_w(z) &= \frac{1}{2}G(0)\gamma_r(z) - \frac{F(0)}{\gamma_r(z)} \\ E(z) &= N\gamma_r(z) + \frac{a_w(0)\gamma_r(z)}{a_w(z)\gamma_0}(E(0)-N\gamma_0)^{1/2} \end{aligned} \tag{12}$$

This should minimize the amount of detrapping.

Figure 2 shows the surface of section obtained by plotting γ versus ψ for 100 particles at the beginning of an FEL section. These phase portraits were obtained by integrating (9) numerically. G and F are held constant for the design corresponding to Fig. 2a. We see a well-defined bucket with electron orbits showing little evidence of stochasticity. In Fig. 2b, G changes linearly with z by 50 percent from one end of the FEL to the other. We now see a very large region of stochasticity. Because G varies rapidly across the induction acceleration unit, the action of trapped orbits jumps every time an induction acceleration unit is traversed. This leads to chaos and detrapping. In both cases the taper $\Delta\gamma \equiv \gamma_r(z=0) - \gamma_r(z=L) = 4$. We have run numerical simulations of many FEL designs (all with linear tapers), and fixing G and F maximizes the

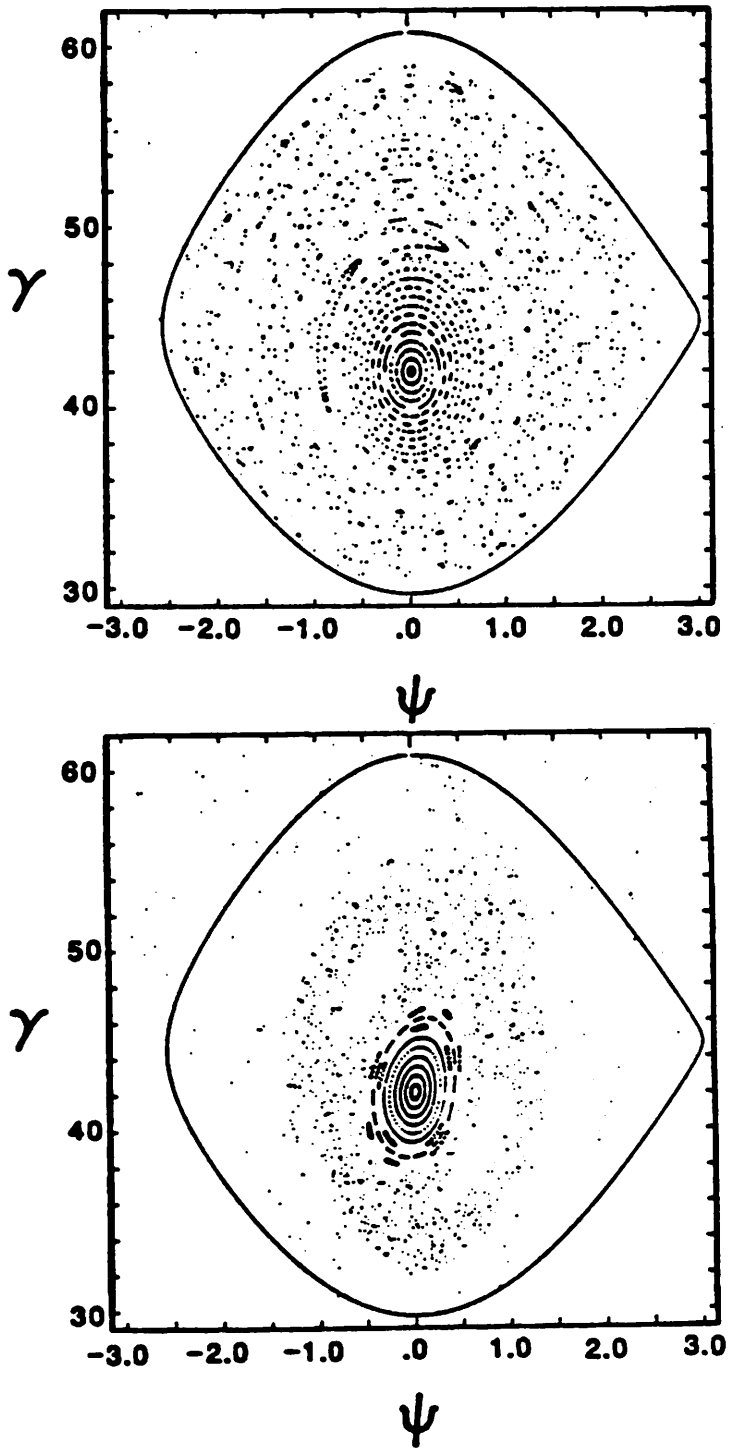

Figure 2: Surface of section plots, γ vs. ψ. a) G and F held constant. b) G varies linearly with z by 50 percent.

size of the trapped region. Allowing G and F to vary by $10-20$ percent leads to trapped regions about 5 percent smaller than in Fig. 2a.

STOCHASTICITY CRITERION

Choosing G and F to be constants, we now estimate the size of the trapped region. The maximum trapped region is defined by the area enclosed by the separatrix, the boundary between libration and rotation around the resonant orbit. For a tapered FEL, the Hamiltonian describing the system is non-autonomous, and we expect the homoclinic orbits forming the separatrix to break up and cross, leading to chaos and detrapping. Effectively, there are two degrees of freedom: the motion of the particles librating in the bucket, and the periodic (period L) forcing of the taper and induction acceleration unit. The interaction between these two degrees of freedom leads to resonances.

The analysis is simplified by employing action-angle variables. The action in a periodic system is defined as

$$J = \frac{1}{2\pi}\oint \gamma d\psi\,. \tag{13}$$

The conjugate angle α is then found by requiring that the transformation from $(\gamma,\psi)\rightarrow(J,\alpha)$ be canonical. This transformation generates a new Hamiltonian of the form

$$K_0(J,z)+K_1(J,\alpha,z)\,. \tag{14}$$

A resonance occurs when the frequencies of the two degrees of freedom are rationally related, so that

$$\frac{\omega_l}{\omega_f}=\frac{r}{s}, \tag{15}$$

where

$$\omega_l(J)=\frac{\partial K_0}{\partial J},\quad \omega_f(L)=\frac{2\pi}{L}. \tag{16}$$

Calculating the location and size of these resonances in phase space allows us to estimate an overlap criterion predicting the size of the chaotic region. Figure 3a is a schematic diagram of the resonances in the (γ,ψ) surface of section. Figure 3b shows the same section in action-angle variables (J,α). We illustrate two sets of resonances, with periods $r/s=5,6$. In a surface of section the periodic orbits appear as fixed points, with an island around each fixed point. Each island has its own separatrix, with higher order resonances forming smaller islands, and so on. This structure is explicated in Lichtenberg and Lieberman[9].

The idea of the overlap criterion is that as the islands grow, their separatrices will touch. When this happens the chaos around each separatrix will link up, destroying any invariant curves that would bound the particle motion. The of overlap is usually parameterized by a stochasticity parameter K[10].

The most convenient approach to the calculation is to construct a surface of section of the flow generated by the Hamiltonian (8). Because the Hamiltonian

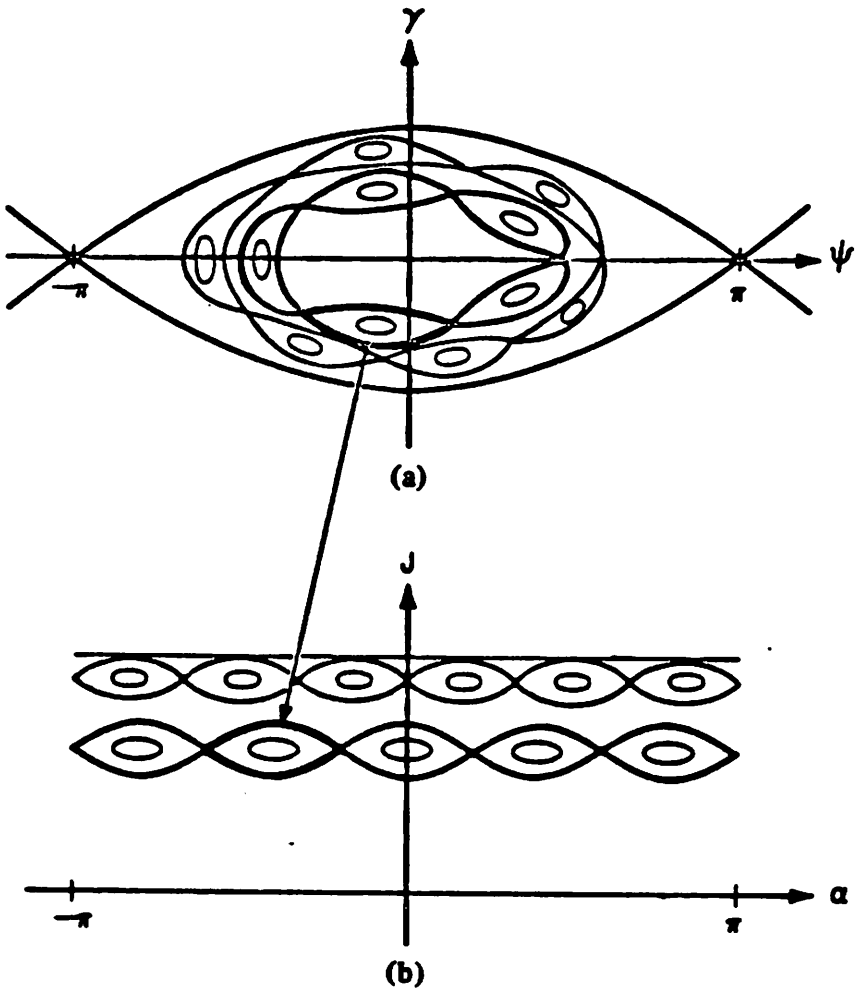

Figure 3: Schematic drawing of the motion near a resonance. Two resonances inside the FEL bucket are shown, a period five and a period six (r/s=5 and 6). a) The (γ, ψ) plane. b) The (J, α) plane.

is periodic in z with period L, we will calculate γ and ψ at $z = nL + \epsilon$, where n is an integer. In this way we will generate a mapping of the phase plane onto itself. Since we are taking an equal time map using canonical variables, Liouville's theorem tells us that the mapping must be area preserving. Starting from the Hamiltonian (11), we expand in powers of ψ. Keeping terms to fourth order in γ and ψ, we obtain

$$\begin{aligned} H = & \frac{1}{2}G\gamma^2 + \frac{1}{2}F\psi^2 - \frac{F}{\gamma_r(z)^2}\gamma^2 - \frac{F_o \sin\psi_r}{\gamma_r(z)}\gamma\psi \\ & - \frac{1}{3!}F_o \sin\psi_r \psi^3 - \frac{1}{2}\frac{F}{\gamma_r(z)}\psi^2\gamma + \frac{F_o \sin\psi_r}{\gamma_r(z)^2}\psi\gamma^2 - \frac{1}{2}[G - \frac{2F}{\gamma_r(z)^2}]\frac{\gamma^3}{\gamma_r(z)} \\ & - \frac{1}{4!}F\psi^4 + \frac{F_o \sin\psi_r}{3!\gamma_r(z)}\psi^3\gamma + \frac{F}{2\gamma_r(z)^2}\psi^2\gamma^2 - \frac{F_o \sin\psi_r}{\gamma_r(z)^3}\gamma^3\psi \\ & + \frac{1}{2}[G - \frac{2F}{\gamma_r(z)^2}]\frac{\gamma^4}{\gamma_r(z)^2} + \ldots \end{aligned} \tag{17}$$

Recall that we have chosen G=const. and F=const. Using the generating function

$$F_1(\psi, \alpha) = 1/2\sqrt{F/G}\psi^2 \cot\alpha \tag{18}$$

to transform to action-angle variables (J, α) of the linearized motion, we obtain the new Hamiltonian

$$\begin{aligned} K &= K_o(J, z) + K_1(J, \alpha, z) \\ &= [\omega_o - \frac{FR}{\gamma_r(z)^2}]J - \frac{1}{16}GJ^2 \\ &\quad - \frac{FR}{\gamma_r(z)^2}J\cos 2\alpha - \frac{F\left(2\sqrt{G/F}\right)^{1/2}}{\gamma_r(z)}J^{\frac{3}{2}}\cos\alpha + \ldots \end{aligned} \tag{19}$$

The $\cos 2\alpha$ term comes from the third term in (17), and the $\cos\alpha$ term comes from the sum of the sixth and eighth terms. We have examined the rest of the terms in (17) and these three (third, sixth, and eighth) contribute the largest jump in the action (the size of which is calculated below). We have defined $\omega_o \equiv \sqrt{GF}$ and $R \equiv \sqrt{F/G}$. The approximate adiabatic invariant (the action) is $J = 1/2\sqrt{G/F}\gamma^2 + 1/2\sqrt{F/G}\psi^2$, while $\alpha = \tan^{-1}\left((F/G)^{1/2}\psi/\gamma\right)$. Treating K_1 as a small perturbation, the zero order motion is

$$\begin{aligned} \frac{dJ_o}{dz} &= 0, \\ \frac{d\alpha_o}{dz} &= \omega - \frac{1}{8}GJ_o \end{aligned} \tag{20}$$

where $\omega = \omega_o - FR/(\gamma_0(\gamma_0 - \Delta\gamma))$, and $\gamma_0 \equiv \gamma_r(0)$. Integrating over one period,

we arrive at the twist mapping

$$\begin{aligned} J_{n+1} &= J_n, \\ \alpha_{n+1} &= \alpha_n + \omega L - \frac{1}{8} GLJ_{n+1}. \end{aligned} \tag{21}$$

This mapping describes the trapped particle motion when there is no taper in the FEL and no induction accelerator kick. The corrections due to these effects are modeled by K_1. To find the corrections to (20), we consider

$$\Delta K = \int_{\epsilon}^{L-\epsilon} \frac{\partial K}{\partial z} dz + \int_{L-\epsilon}^{L+\epsilon} \frac{\partial K}{\partial z} dz = I_1 + I_2. \tag{22}$$

Because of adiabatic invariance we expect the first integral I_1, due to the slow changes in parameters along the FEL, to be small. The second integral I_2 describes the effects of the sudden change in FEL parameters from the end of one FEL to the beginning of the next. If there is any mismatch in the taper $\Delta\gamma$ and the size of the kick in energy imparted by the induction acceleration unit, it would also be included in I_2. Writing out the first integral, we find

$$I_1 = \int_0^L \frac{2FRJ\cos\alpha}{\gamma_r(z)^3} \left(\frac{d\gamma_r}{dz}\right) dz + \int_0^L \frac{\left(2\sqrt{G/F}\right)^2 J^{3/2}\cos\alpha}{\gamma_r^2} \left(\frac{d\gamma_r}{dz}\right) dz. \tag{23}$$

We consider the second term (the first is smaller by a factor $1/\gamma_r \approx 1/40$). We expand

$$\frac{1}{\gamma_r(z)^2} = a_o/2 + \sum_{n=1}^{\infty} a_n \cos\frac{2\pi nz}{L} + b_n \sin\frac{2\pi nz}{L} \tag{24}$$

where

$$\begin{aligned} a_n &\approx \frac{12}{\gamma_r(0)^2} \left(\frac{\Delta\gamma}{2\pi\gamma_r(0)}\right)^2 \frac{1}{n^2} + \ldots \\ b_n &\approx \frac{4}{\gamma_r(0)^2} \left(\frac{\Delta\gamma}{2\pi\gamma_r(0)}\right) \frac{1}{n} + \ldots \end{aligned} \tag{25}$$

Then we can estimate the size of I_1 by

$$\begin{aligned} I_1 &= \left(2\sqrt{G/F}\right)^{1/2} F J_n^{3/2} \left(\frac{4\Delta\gamma}{2\pi m\gamma_r(0)^3}\right) \cos\alpha_n + \ldots \\ &= d_m J_{n+1} \cos\alpha_n + \ldots \ . \end{aligned} \tag{26}$$

for a resonance of order $r/s = m$ ($s = 1$ leads to the largest effect). Away from

resonance the integral is much smaller. Now consider I_2:

$$\begin{aligned} I_2 &= -FRJ_{n+1}\cos 2\alpha_n \int_{L-\epsilon}^{L+\epsilon} \frac{d}{dz}\left(\frac{1}{\gamma_r(z)^2}\right) dz \\ &\quad - \left(2\sqrt{G/F}\right)^{\frac{1}{2}} FJ_{n+1}^{\frac{3}{2}} \cos\alpha_n \int_{L-\epsilon}^{L+\epsilon} \frac{d}{dz}\left(\frac{1}{\gamma_r(z)}\right) dz \\ &= -FRJ_{n+1}\cos\alpha_n \left[\frac{1}{\gamma_o^2} - \frac{1}{(\gamma_o - \Delta\gamma)^2}\right] \\ &\quad + \left(2\sqrt{G/F}\right)^{\frac{1}{2}} FJ_{n+1}^{\frac{3}{2}} \cos\alpha_n \frac{\Delta\gamma}{\gamma_0(\gamma_0 - \Delta\gamma)} \\ &= a\omega J_{n+1}\cos 2\alpha_n + b\omega J_{n+1}^{\frac{3}{2}} \cos\alpha_n. \end{aligned} \tag{27}$$

We have defined the small quantities

$$\begin{aligned} a &= -\frac{FR}{\omega}\left[\frac{1}{\gamma_o^2} - \frac{1}{(\gamma_o - \Delta\gamma)^2}\right] \\ b &= \left(2\sqrt{G/F}\right)^{\frac{1}{2}} \left[\frac{F}{\omega}\right] \frac{\Delta\gamma}{\gamma_0(\gamma_0 - \Delta\gamma)}. \end{aligned} \tag{28}$$

For $\gamma_0 = 42$, $\Delta\gamma = 4$, $a_w = 13$ and $a_s = 0.4$, the nominal design values, we find $a \approx 7\times10^{-3}$ and $b \approx 1\times10^{-2}$. For the same design values we have $d_m \approx 3\times10^{-7}$. Thus for the tapers envisioned for use in the TBA we may neglect the change in action due to the non-adiabaticity of J in the FEL. The result is, using just I_2,

$$\Delta K = \omega a J_{n+1}\cos 2\alpha_n + \omega b J_{n+1}^{3/2}\cos\alpha_n. \tag{29}$$

To see how this affects the mapping, observe that

$$\begin{aligned} \Delta K_n &= K(nL+\epsilon) - K\left((n-1)L+\epsilon\right) \\ &= \omega(J_{n+1} - J_n) - (G/8)(J_{n+1} - J_n)J_n + O(\Delta J^2). \end{aligned} \tag{30}$$

For trapped particles $(G/8)J_n << \omega$ so we neglect that term. Then from (30) $\Delta J = (\Delta K/\omega)$ and the first order change in J becomes

$$J_{n+1} = J_n + aJ_{n+1}\cos 2\alpha_n + bJ_{n+1}^{3/2}\cos\alpha_n. \tag{31}$$

This change in J is derivable from the generating function

$$F_2(J_{n+1},\alpha_n) = J_{n+1}\alpha_n + \omega L J_{n+1} - \frac{a}{2}J_{n+1}\sin 2\alpha_n - bJ_{n+1}^{\frac{3}{2}}\sin\alpha_n \tag{32}$$

through the equation $J_{n+1} = \partial F_2/\partial\alpha_n$. Using $\alpha_{n+1} = \partial F_2/\partial J_{n+1}$, we obtain the change in α_n to first order, which yields the complete mapping

$$\begin{aligned} J_{n+1} &= J_n + aJ_{n+1}\cos 2\alpha_n + bJ_{n+1}^{3/2}\cos\alpha_n\,, \\ \alpha_{n+1} &= \alpha_n + \omega L - \frac{1}{8}GJ_{n+1}L - \frac{a}{2}\sin 2\alpha_n - \frac{3}{2}bJ_{n+1}^{\frac{1}{2}}\sin\alpha_n. \end{aligned} \tag{33}$$

To find the stochasticity condition, we note that we are interested in motion near the separatrix, where $J >> 1$, so that $a << b\sqrt{J} << GLJ$. Hence we set $a = 0$. Then we define $I = -(1/8)GLJ$ to obtain

$$\begin{aligned} I_{n+1} &= I_n + K(J)cos\alpha_n\,, \\ \alpha_{n+1} &= \alpha_n + \omega L + I_{n+1} + \ldots \end{aligned} \tag{34}$$

where $K(J) = GLbJ^{3/2}/8$ is the stochasticity parameter and we neglect the term involving $b\sqrt{J} << GLJ$ in the α equation. This is a slight generalization of Chirikov's standard map[10]. Setting $K = .976 \approx 1$ to find the island overlap condition, we obtain

$$K_{crit} = \frac{GL}{8} b J_{crit}^{\frac{3}{2}} = 1. \tag{35}$$

The action at which the motion becomes stochastic is then

$$J_{crit} \approx \left[\frac{8\omega\gamma_0(\gamma_0 - \Delta\gamma)}{FGL(2\sqrt{G/F})^{1/2}\Delta\gamma}\right]^{\frac{2}{3}} \tag{36}$$

We note that $J_{crit} \to \infty$ as $\Delta\gamma \to 0$, meaning that the entire bucket is regular. Of course the estimate (36) only makes sense for $J_{crit} \leq J_{sx} \approx (8/\pi)\sqrt{F/G}$, the action of the separatrix orbit. If this inequality holds, the fraction of the bucket filled by trapped orbits is

$$\frac{J_{crit}}{J_{sx}} = \left(\frac{1}{2^{4/3}\pi F^{2/3}}\right)\left[\frac{\gamma_0(\gamma_0 - \Delta\gamma)}{\Delta\gamma}\right]^{2/3}. \tag{37}$$

Writing F in terms of the FEL parameters, we obtain from (37) the explicit result

$$\frac{J_{crit}}{J_{sx}} = \left(\frac{1}{2^{4/3}\pi\left((\omega_s a_w(0)a_s(0)/\gamma_0 c)^2 - \Delta\gamma^2/L^2\right)^{1/3}}\right)\left[\frac{\gamma_0(\gamma_0 - \Delta\gamma)}{\Delta\gamma}\right]^{2/3}. \tag{38}$$

As $\Delta\gamma$ is increased the stochastic region around the separatrix grows into the trapped region and J_{crit} decreases. Figure 4 is a plot of the ratio (trapped area/bucket area) versus taper $\Delta\gamma$. The solid line is the prediction of (37). The points are measurements of the maximum deviation of γ in the trapped region from the resonant value taken from numerical integrations of (9). These are converted to a ratio of areas, trapped area divided by the area inside the separatrix, by ratio= $(\gamma_{max}/\gamma_{sx})^2$. There are two points at each taper since the ratios for γ at the top of the bucket and at the bottom differ slightly. For small tapers our calculation predicts perfect trapping. The numerical experiments indicate very little detrapping in agreement with the theory. Around $\Delta\gamma =$ 15, where our calculation predicts detrapping, the area of the trapped region observed in the numerical experiments rapidly decreases.

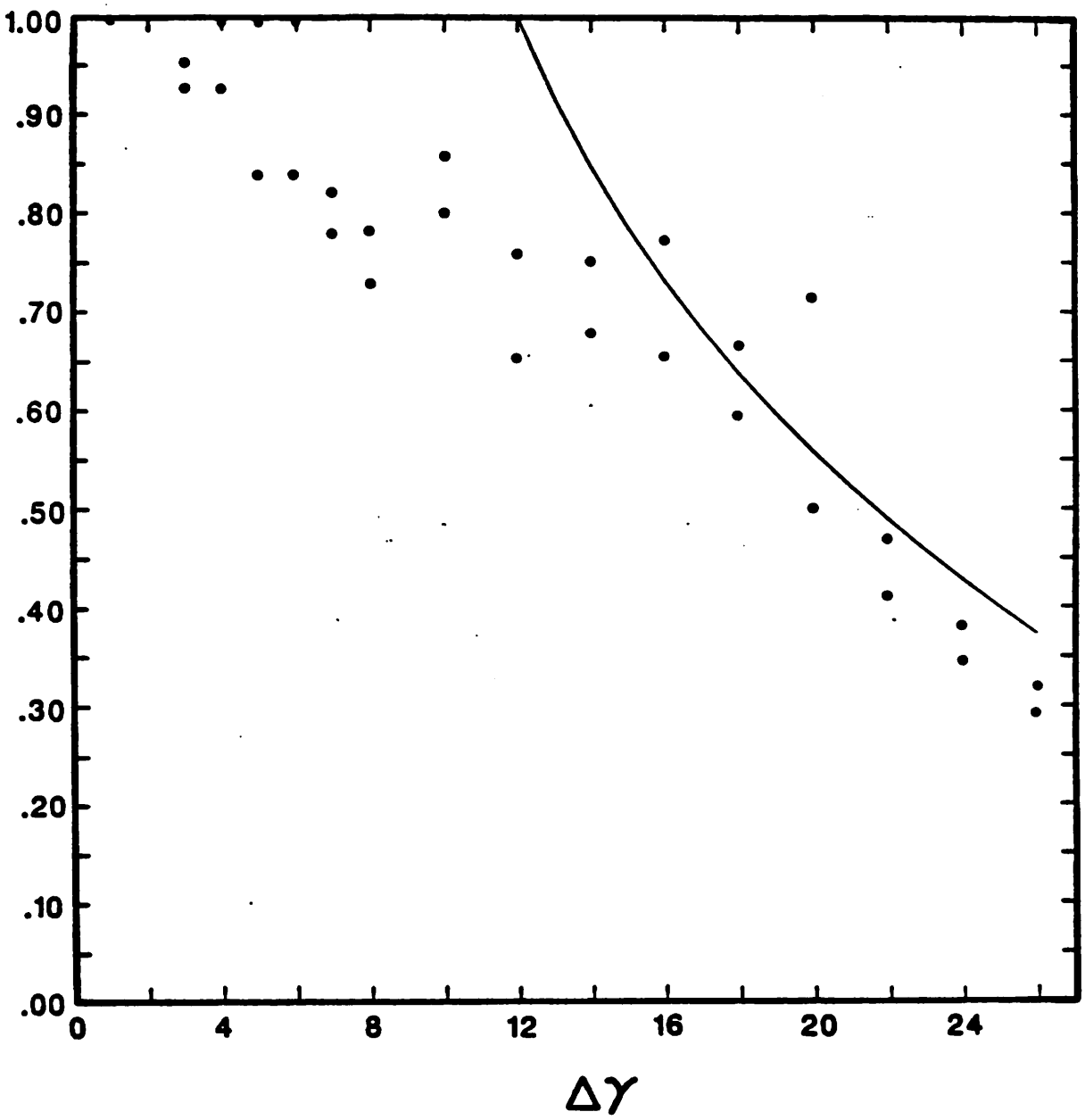

Figure 4: Size of the trapped region at the beginning of an FEL section. The solid line is the prediction of the overlap criterion. The dots are from numerical integrations. Here $\gamma_r = 42$.

RESONANT ISLANDS

The mapping (33) that we have derived gives us more information about orbits than the simple stochasticity criterion. Fixed points of the mapping correspond to closed, periodic orbits of the flow in phase space. To see this, consider the Hamiltonian (8), modified to take into account the energy extracted from the FEL:

$$H(\gamma,\psi,E,\chi)=\sum_{i=1}^{N}\Bigg\{k_w((\gamma_r+\gamma_i))+\frac{\omega_s}{2c(\gamma_r+\gamma_i)}((1+a_w^2))- \frac{k_p a_w}{(\gamma_r+\gamma_i)}\frac{(E-N\gamma_r)^{1/2}}{N^{1/2}}\cos(\psi_r+\psi_i)+\frac{d\gamma_r}{dz}\psi_i-f(z)\chi\,. \tag{39}$$

The energy E evolves independently of the rest of the dynamics, since $dE/dz = f(z)$ is fixed by the design. Also, the evolution of χ does not influence the evolution of γ or ψ. The problem reduces to a one degree of freedom, "time" (z) dependent system. All orbits start at $z = 0$ and evolve to $z = 500L$. However, since each FEL-inductor pair is identical we may identify axial positions that differ by L. Identifying points with z coordinate differing by L means that the flow is on a torus. The mapping is a slice through the torus at a particular value of z mod L. Orbits that return to the same values of γ and ψ in this slice are closed orbits.

We expect the topology of the flow to be affected by the presence of stable or unstable periodic orbits. In particular, we know that islands exist around stable periodic orbits, and that particles initially in such an island will be trapped in that island. Thus, we expect particles to be trapped around a stable periodic orbit inside the trapped region of the FEL bucket. If the island is large, a significant number of particles will be trapped in orbits that remain close to the periodic orbit. These particles will rotate around γ_r and ψ_r in a coherent manner, behaving as if they were one large particle. Such a super particle, if large enough, might alter the signal wave in a deleterious manner. Figure 5 is a section taken 15 cm along the FEL, showing several such islands surrounding the main resonance.

We use the mapping (33) to calculate the location in phase space of periodic orbits, the stability of such orbits, and the size of any island around a stable periodic orbit. To find orbits with period L, we set $\Delta J = J_{n+1} - J_n = 0$ and $\Delta\alpha = \alpha_{n+1} - \alpha_n = 2\pi q$, where q is an integer. Writing $g(J,\alpha;L)$ for $(\Delta J, \Delta\alpha)$, we set

$$g(J,\alpha;L)=\begin{pmatrix} aJ\cos 2\alpha + bJ^{\frac{3}{2}}\cos\alpha \\ (\omega-\frac{1}{8}GJ)L-\frac{a}{2}\sin 2\alpha-\frac{3}{2}bJ^{\frac{1}{2}}\sin\alpha-2\pi q\end{pmatrix}=0. \tag{40}$$

We think of L as a bifurcation parameter. A necessary condition for a bifurcation is that the eigenvalues of Dg lie on the unit circle:

$$Dg=\begin{pmatrix} A & A\frac{\partial\Delta J}{\partial g} \\ A\frac{\partial\Delta\alpha}{\partial J} & A^{-1}+A\frac{\partial\Delta\alpha}{\partial J}\frac{\partial\Delta J}{\partial\alpha}\end{pmatrix} \tag{41}$$

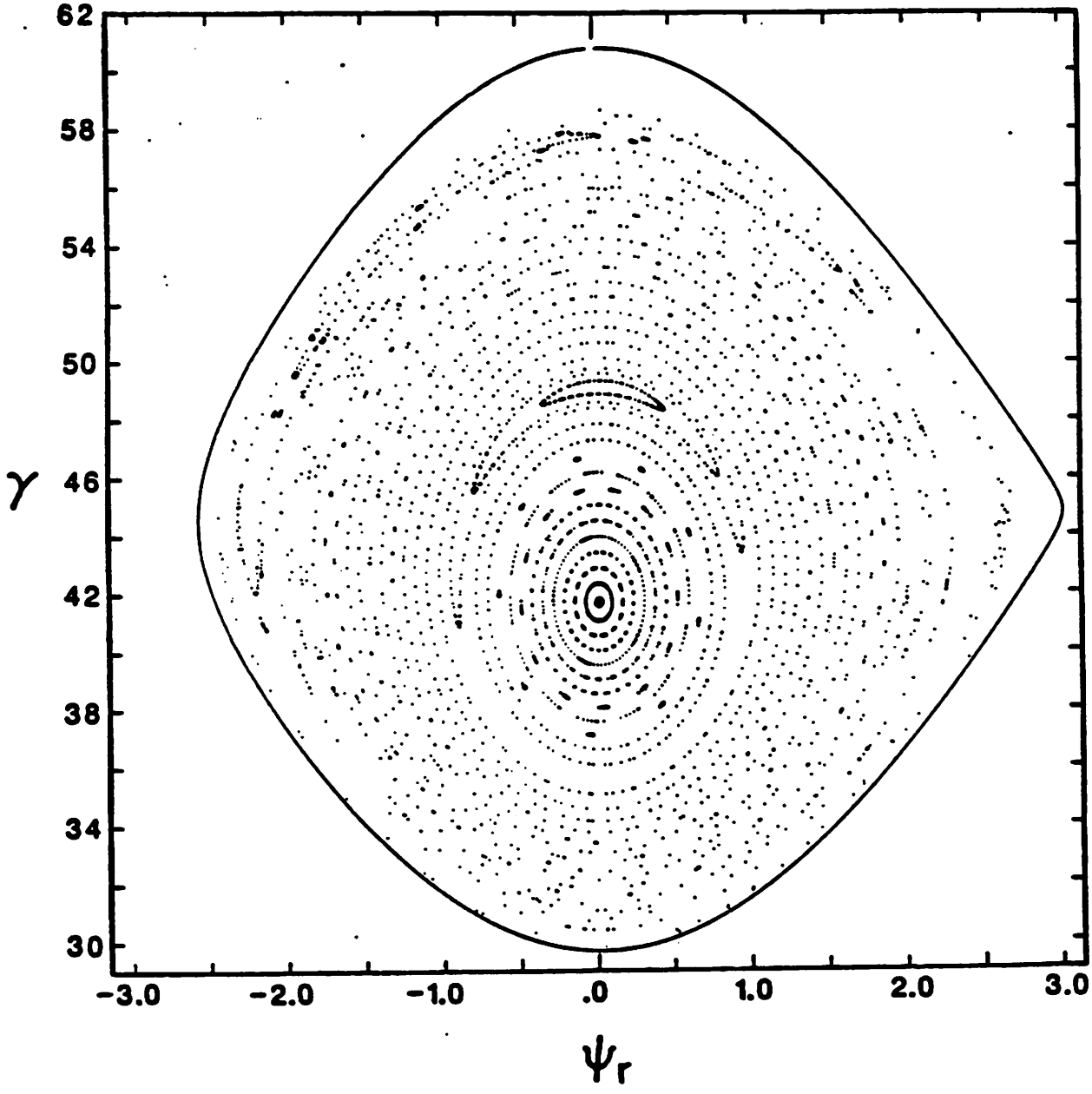

Figure 5: Surface of section plot of γ vs. ψ, 15 cm along the FEL. Compare to Fig. 2a

where

$$\begin{aligned} A =& \frac{\partial J_{n+1}}{\partial J_n} \\ =& \frac{1}{(1 - a\cos 2\alpha - (3/2)bJ^{1/2}\cos\alpha)}, \\ \frac{\partial \Delta J}{\partial \alpha} =& -2a\sin 2\alpha - bJ^{3/2}\sin\alpha, \\ \frac{\partial \Delta \alpha}{\partial J} =& -\frac{1}{8}GL - \frac{3b}{4\sqrt{J}}\sin\alpha. \end{aligned} \tag{42}$$

If we look for bifurcation of the central fixed point at $J = 0$, $\partial\Delta J/\partial\alpha \to O(J)$, $\partial\Delta\alpha/\partial J \to O(1/\sqrt{J})$ and $A = 1/(1 - a\cos 2\alpha)$. The eigenvalues are $\lambda_1 = 1 - a\cos 2\alpha$ and $\lambda_2 = 1/(1 - a\cos 2\alpha)$. Setting $\lambda = 1$ fixes $\alpha = \pm\pi/4, \pm 3\pi/4$. Since α must be fixed $g(J_b, \alpha_b; L) = 0$ may be solved for

$$L_{\pm} = \frac{4\pi q \pm a}{2\omega}. \tag{43}$$

The plus sign corresponds to $\alpha = \pi/4$ and $-3\pi/4$, while the minus sign corresponds to $\alpha = -\pi/4$ and $3\pi/4$. In both cases there is a collision between two orbits which exchange stability. In the collision at $L_- = 4\pi q - a/(2\omega)$ the stable fixed point at $J = 0$ loses stability to an unstable fixed point born at a slightly smaller L,

$$L_{T1} \approx L_- \left(1 - \frac{9b^2}{G(4\pi q - a)}\right), \tag{44}$$

in a saddle-node bifurcation. In the collision at $L = 4\pi q + a/(2\omega)$ the unstable fixed point at $J = 0$ regains stability after colliding with a stable orbit born in a second saddle-node bifurcation at

$$L_{T2} \approx L_+ \left(1 - \frac{9b^2}{G(4\pi q + a)}\right). \tag{45}$$

Finally there is a third saddle-node bifurcation in which the stable fixed point originating at $J = 0$, $\alpha = 3\pi/4$, $L = L_-$ annihilates the unstable fixed point which originated in the collision at $J = 0$, $\alpha = -3\pi/4$, $L = L_+$. This occurs at $J \approx a^2/b^2$, $\alpha \approx \pm\pi$, $L_{T3} \approx (2\pi q + a/2)/(\omega - (1/8)Ga^2/b^2)$. The bifurcation diagram and the corresponding phase spaces are shown in Fig. 6.

The result of all these bifurcations is that one stable island is born at small positive J and moves to larger J as L increases. At the center of the island is a fixed point located at (J_q, α_q). From (40) we find for $J_q > 4a/(GL) \approx .01$

$$\begin{aligned} J_q &\approx \frac{8}{G}\left(\omega - \frac{2\pi q}{L}\right), \\ \alpha_q &\approx \frac{\pi}{2} - \frac{2a}{b\sqrt{J_q}}. \end{aligned} \tag{46}$$

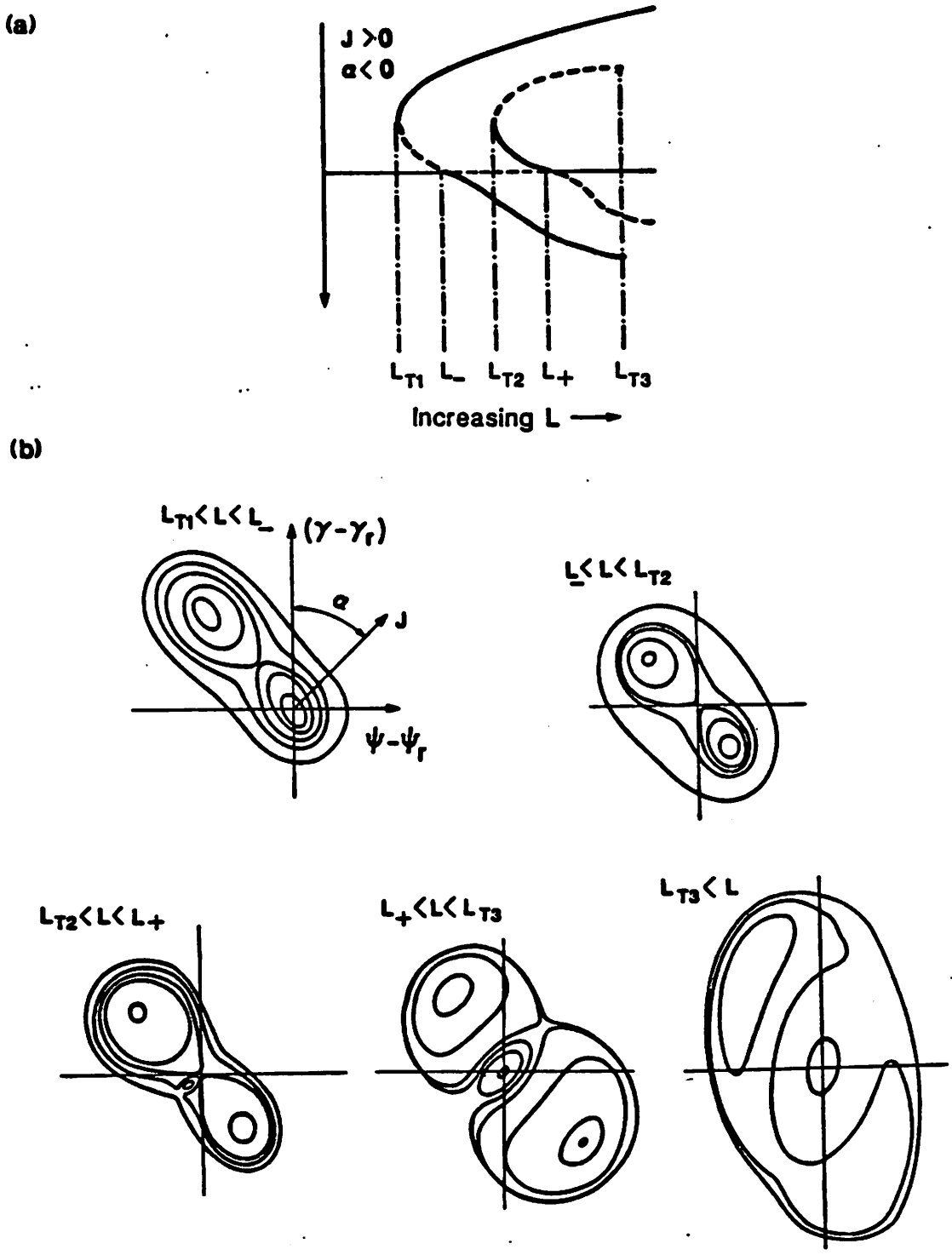

Figure 6: Bifurcation diagram for the TBA. a) Location of the stable (solid lines) and unstable (dashed lines) fixed points as a function of L. b) Phase space portraits for values of L marked in a).

We are treating the zero order problem as if it were a harmonic oscillator rather than a pendulum. This simplifies the analysis but the price we pay is that the frequency $\omega(J) = \omega_o - (1/8)GJ$ does not go to zero at the separatrix. In fact our $\omega(J)$ is too large for all non-zero values of J. This means that our predicted value of J_q, and hence ψ_q, will be too large. This small but noticeable error can be reduced by using the full pendulum Hamiltonian as the zero order system. The resulting action and frequency, involving elliptic integrals, are given in [9], for example.

We are interested in the area of the island and its amplitude of oscillation $\delta\gamma$ about γ_r. We note that $\delta\gamma$ is proportional to $\sqrt{J}$. If $\delta\gamma$ is small there will be no noticeable oscillations in a_s since in that case the coherent motion will not change the average energy of the beam. Therefore we consider only the case $J_q >> 1$. To find the area of the island, we linearize around the fixed point at (J_q, α_q). Ignoring the term proportional to J since $J^{3/2} >> J$, we find

$$\begin{aligned} \delta J_{n+1} &= \delta J_n + b J_q^{\frac{3}{2}} \sin \delta\alpha_n \\ \delta\alpha_{n+1} &= \delta\alpha_n - \frac{1}{8} GL \delta J_{n+1}. \end{aligned} \tag{47}$$

Letting $I = (GL/8)J$ we arrive at the standard map[10] with $K = (1/8)GLbJ^{3/2}$. The width of the island in the standard map is $2\sqrt{K}$, or

$$\Delta I_m = 2\sqrt{\frac{GLbJ_q^{\frac{3}{2}}}{8}}. \tag{48}$$

In terms of J

$$\Delta J_m = \sqrt{\frac{32b}{GL}} J_q^{\frac{3}{4}}. \tag{49}$$

The width ΔJ_m is a function of the taper of the wiggler through b, and depends explicitly on the length of the FEL. We may compare this calculation to the results of numerical integration of the basic equations (9). The results are shown in Fig. 7. Figure 7a is a plot of $\psi_q = \sqrt{2J_q/R}\sin\alpha_q$ as a function of the length of the FELs. (The fixed point is at $\gamma_q \approx 0$ so we plot only ψ_q). The taper of the wiggler is four. The data points are taken from surface of section plots like those in Fig. 5, obtained by integrating (9). The solid line is the prediction of (46).

Figure 7b gives the width $\Delta\psi$ of the island in radians as a function of the length of the FELs. The solid line is found using (49) and the canonical transformation from (J, α) to (γ, ψ), and the points are measurements from phase plots. The area of the island around the stable fixed point may be an appreciable fraction (8 to 10 percent) of the area of the trapped region. Particles inside this island will oscillate coherently around the center of the trapped region. They oscillate (nearly) as a rigid body around (γ_r, ψ_r) with

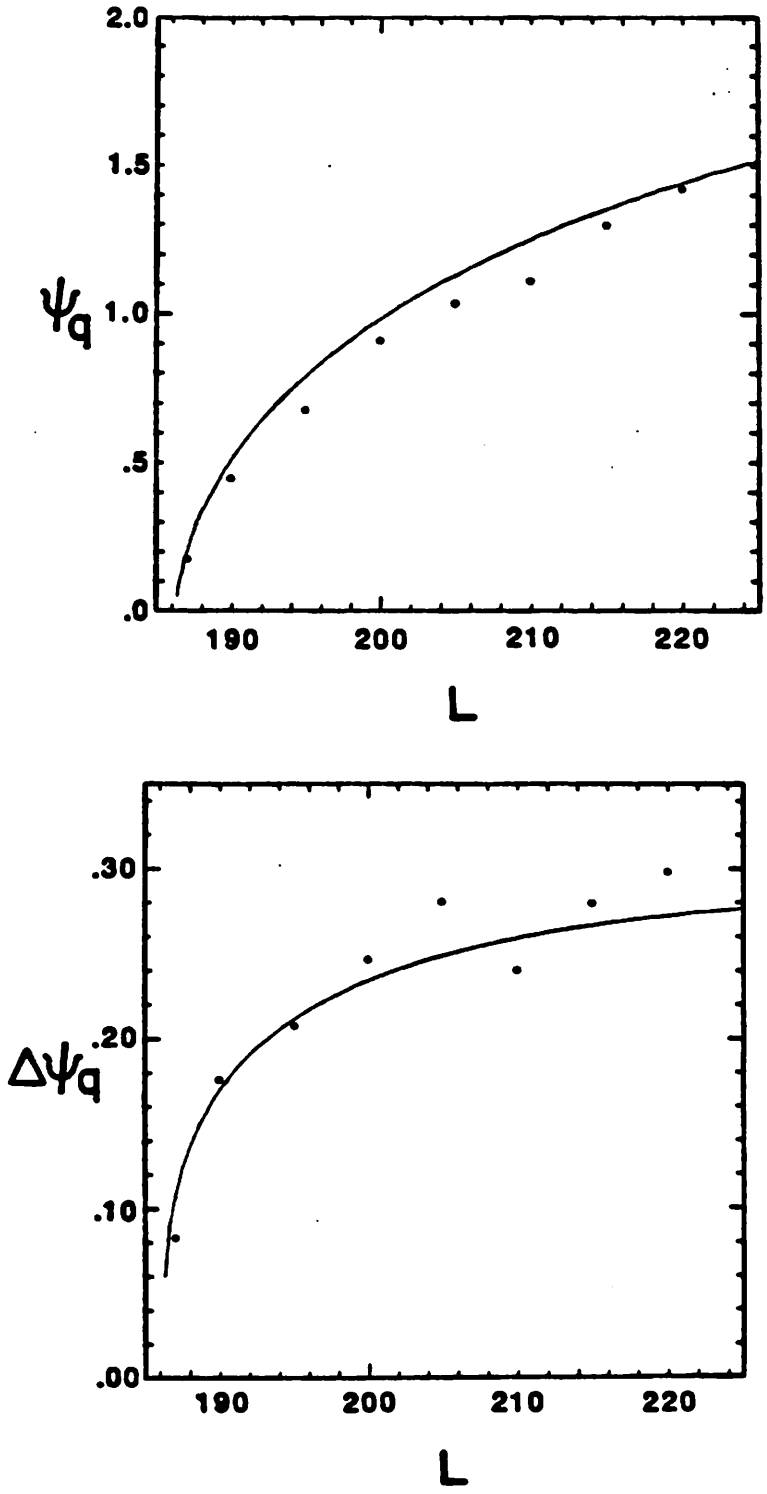

Figure 7: Superparticle island location and size as a function of L. a) ψ_q vs. L. The solid line is the prediction of the mapping. The dots are data from surface-of-section plots. b) Width of island $\Delta\psi_q$ vs. L.

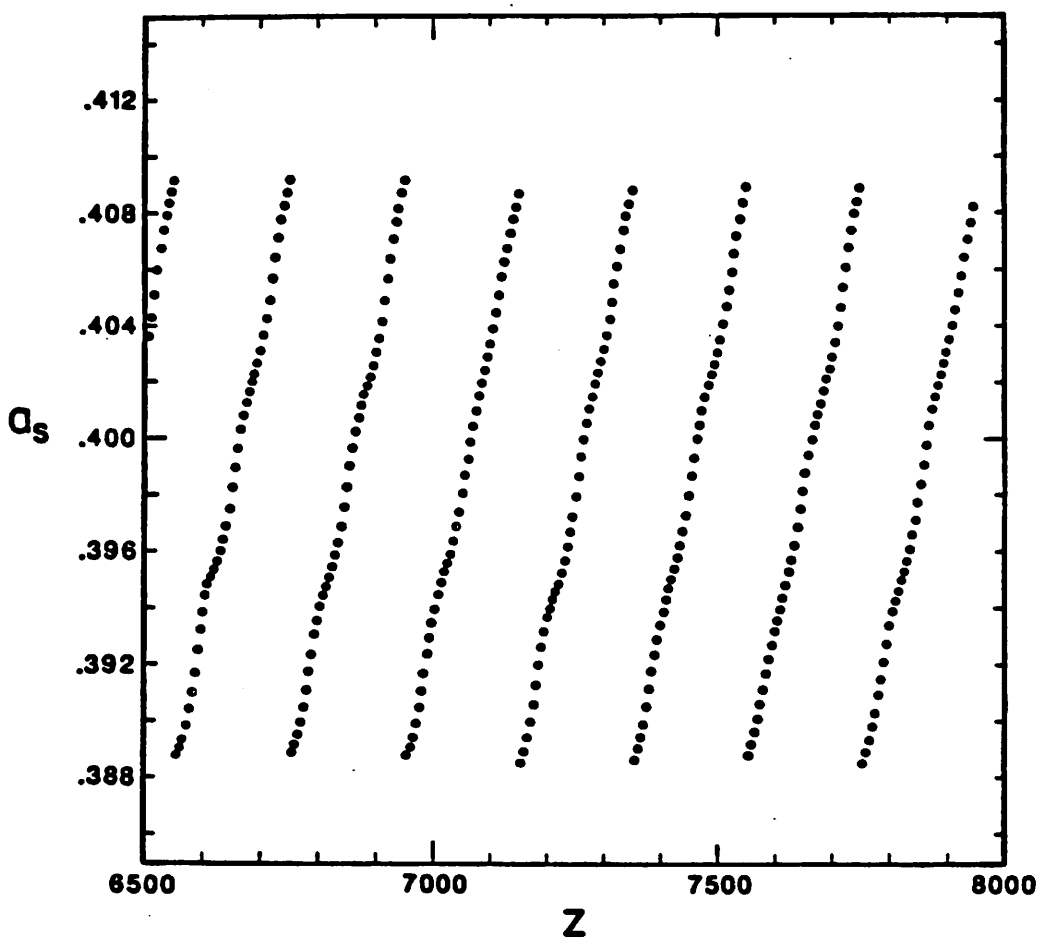

Figure 8: Signal amplitude a_s as a function of z.

the frequency corresponding to J_q, that is, $\omega = 2\pi q/L$. This coherent motion will modulate a_s, causing it to oscillate around its nominal value (Fig. 8). This will produce a modulation in ϕ, the phase of the signal, adversely affecting the acceleration of the high energy beam. In addition, the modulation introduces another frequency into the FEL which may drive parametric instabilities.

One way to alleviate this problem is suggested by Fig. 7. We can adjust the length of the FEL (or ω) so that the islands born in bifurcations are either out near the separatrix or near the central fixed point. Particles in islands near the separatrix will be detrapped so that there is little coherent motion. At the same time L must be chosen so that the most recently born island is near the center of the bucket. This will have two effects. First, the area of the island will be small, so that the number of coherently rotating particles is small. Second, the amplitude of oscillation $\delta\gamma$ is small, so that a_s is not strongly modulated. In Fig. 2, J_1 and J_2 are near the separatrix, but J_3 is too large and causes the oscillations shown in Fig. 8.

CONCLUSIONS

We have studied a simple one dimensional model to examine the performance of the two beam accelerator. In order for the accelerator to be successfully operated the electrons that drive the FELs must be trapped in the ponderomotive potential well bucket. Because the TBA employs tapered FELs the particle motion is described by a non-autonomous one degree of freedom Hamiltonian. In general the Hamiltonian predicts stochastic motion leading to detrapping of particles. This detrapping is observed in numerical integrations of the equations describing the TBA, at a level in agreement with theoretical predictions. We have given a criterion to keep the detrapping to acceptable levels.

Resonances between the nonuniform spatial dependence and the libration of particles in the FEL bucket lead to the formation of islands within the bucket. These islands trap particles in the same manner that the bucket does. Such island particles rotate coherently within the well, modulating the power output of the FELs. We have determined the position and size of the islands in phase space. Suitable choices of parameters allows us to minimize the amplitude of the modulation.

We conclude that if the design of the FELs employed in the TBA is suitably chosen, stochasticity and detrapping will not significantly degrade the performance of the TBA.

ACKNOWLEDGMENTS

This work was supported by National Science Foundation Contract No. ECS 8517364 and by U.S. Office of Naval Research Contract N00014-84-K-0367. Numerical work was done on the National Magnetic Fusion Energy Computer Center (NMFECC) computer network.

REFERENCES

1. B. Richter, "Requirements For Very High Energy Accelerators", in **Laser Acceleration of Particles**, C. Joshi and T. Katsouleas ed., (AIP Conference Proceedings No. 130, N. Y.,1985) p. 8.

2. P. B. Wilson, IEEE Trans. on Nuclear Science, NS-28, 2742 (1981)

3. A. M. Sessler, "The Free Electron Laser as a Power Source for a High Gradient Structure", in **Laser Acceleration of Particles**,P. J. Channel ed., (AIP Conference Proceedings No. 91, N. Y., 1982), p. 163.

4. D. Prosnitz, IEEE Trans. on Nuclear Science, NS-30, 2754 (1983)

5. J. S. Wurtele, "On Acceleration by the Transfer of Energy Between Two Beams", in **Laser Acceleration of Particles**, C. Joshi and T. Katsouleas eds. (AIP Conference Proceedings No. 130, N. Y., 1985), p. 305.

6. D. B. Hopkins, A. M. Sessler, and J. S. Wurtele, Nucl. Instr. and Meth. in Phys. Res. **228**, 15 (1984).

7. E. Sternbach, and A. M. Sessler, Lawrence Berkeley Laboratory report LBL-19939, and private communication.

8. N. M. Kroll, P. L. Morton, M. W. Rosenbluth, IEEE Journal of Quantum Electronics, **QE 17**, 1436 (1981).

9. A. J. Lichtenberg and M. A. Lieberman, *Regular and Stochastic Motion* (Springer-Verlag N. Y., 1983)

10. B. V. Chirikov, Phys. Rep. **52** No. 5 263 (1979)